

Generation of ductal organoids from normal mammary luminal cells reveals invasive potential

Hilary M Ganz^{1*}, Benedikt Buchmann^{2†}, Lisa K Engelbrecht^{2†}, Moritz Jesinghaus^{3,4}, Laura Eichelberger^{5,6}, Christian J Gabka⁷, Georg P Schmidt⁸, Alexander Muckenhuber³, Wilko Weichert^{3,9}, Andreas R Bausch² and Christina H Scheel^{1,10*}

¹ Institute of Stem Cell Research, Helmholtz Center for Health and Environmental Research Munich, Neuherberg, Germany

² Chair of Cellular Biophysics E27, Technical University Munich, Garching, Germany

³ Institute of Pathology, Technical University of Munich, Munich, Germany

⁴ Institute of Pathology, University Hospital Marburg, Marburg, Germany

⁵ Center for Functional Protein Assemblies, Technical University of Munich, Munich, Germany

⁶ Clinic and Polyclinic for Internal Medicine II, Klinikum rechts der Isar, Technical University of Munich, Munich, Germany

⁷ Nymphenburg Clinic for Plastic and Aesthetic Surgery, Munich, Germany

⁸ Department of Obstetrics and Gynecology, Klinikum rechts der Isar, Technical University of Munich, Munich, Germany

⁹ German Cancer Consortium (DKTK), Partner Site Munich, Munich, Germany

¹⁰ Department of Dermatology, St. Josef Hospital, Ruhr-University Bochum, Bochum, Germany

*Correspondence to: HM Ganz, Institute of Stem Cell Research, Helmholtz Center for Health and Environmental Research Munich, Ingolstädter Landstraße 1, 85764 München, Germany. E-mail: hilary.ganz@tum.de; or CH Scheel, Department of Dermatology, Ruhr-University Bochum, Gudrunstr. 56, 44791 Bochum, Germany. E-mail: christina.scheel@klinikum-bochum.de

†These authors contributed equally to this work.

Abstract

Here we present an experimental model for human luminal progenitor cells that enables single, primary cells isolated from normal tissue to generate complex branched structures resembling the ductal morphology of low-grade carcinoma of no special type. Thereby, we find that ductal structures are generated through invasive branching morphogenesis via matrix remodeling and identify reduced actomyosin contractility as a prerequisite for invasion. In addition, we show that knockout of E-cadherin causes a dissolution of duct formation as observed in invasive lobular carcinoma, a subtype of invasive carcinomas where E-cadherin function is frequently lost. Thus, our model shows that invasive capacity can be elicited from normal luminal cells in specific environments, which results in low-grade no special type morphology. This assay offers a platform to investigate the dynamics of luminal cell invasion and unravel the impact of genetic and non-genetic aberrations on invasive morphology.

© 2021 The Authors. *The Journal of Pathology* published by John Wiley & Sons, Ltd. on behalf of The Pathological Society of Great Britain and Ireland.

Keywords: primary human mammary epithelial cells; luminal progenitor (LP) cell; invasive breast cancer; apical-basal polarity; organoid; ductal; branching morphogenesis

Received 10 March 2021; Revised 12 August 2021; Accepted 28 August 2021

Conflict of interest statement: The authors declare no competing financial interests. HMG, CHS, LKE, ARB, and BB are inventors on a patent application based on the presented assay.

Introduction

The mammary gland consists of a bilayered branched epithelial network with an inner layer of luminal cells and an outer layer of myoepithelial/basal cells. Breast cancer is thought to generally arise from the luminal epithelial cells [1–4]. Highly proliferative cancerous cells can either remain within the confined luminal spaces (*in situ* carcinomas) or breach the basal cell layer and lamina, resulting in invasive breast carcinomas [5]. There are several morphologically distinct types of

invasive carcinoma. The most commonly diagnosed type is invasive carcinoma of no special type (NST), also known as invasive ductal carcinoma, which comprises over 70% of all cases [6]. Histologic grade of NST is, among other factors, determined based on the extent to which cancer cells form differentiated ducts, a measurement that bears prognostic value [7–10]. Thereby, arising ducts resemble normal mammary gland morphology, but they consist solely of invasive luminal cells that maintain expression of luminal markers such as GATA3 [11,12] and specific

cytokeratins [13]. In this grading system, a high degree of well-differentiated ductal network formation is attributed to low-grade disease [10]. Importantly, certain genetic aberrations have a direct impact on mammary duct formation. One prominent example is E-cadherin, which is typically lost in invasive lobular carcinomas (ILC), a subtype where duct formation is completely absent [14,15].

Understanding the mechanisms that underlie invasive outgrowth of epithelial cells holds the key to the prevention of invasive breast cancer. Importantly, so far it has not been possible to identify universal genetic alterations that distinguish pre-invasive from invasive carcinomas [16–18]. Recent single-cell analyses support these findings by showing that rather than being driven by one or a few dominant clones, a variety of clones invade concomitantly [19,20]. This lack of support for specific genetic determinants of invasion might indicate that a conserved mechanism for invasive growth is already present within pre-invasive luminal cells and that the process of invasion is influenced by the microenvironment or tumor stroma [21,22]. This fits with the perception that basal cells and basal lamina act as a physical, invasion-suppressing barrier between luminal cells and extracellular matrix (ECM) [23–25]. However, during invasive cancer development, this barrier loses its integrity, allowing direct contact of luminal cells with the ECM [23,24,26,27]. The main structural component of the human mammary ECM is collagen type I, which is even more predominant in invasive carcinomas [28]. *In vivo*, collagen type I can drive tumor cell invasion [29,30]. In addition, collagen type I has been shown to encourage invasive behavior and support branching morphogenesis *in vitro* in epithelial cells, including the basal mammary epithelial subset [31–33]. In analogy, invasive growth could be elicited from luminal cells once they converted towards a basal phenotype [34]. However, collagen-induced invasive branching morphogenesis resulting in the ductal morphology that is characteristic for NST carcinomas has so far not been observed in luminal cells *in vitro*. Instead, human luminal progenitor (LP) cells cultivated in collagen type I gels in a manner where their luminal identity was maintained were shown to grow out into spheres or budding-like structures [33] with reversed apical-basal polarity [35]. Consequently, 3D models of invasive growth have relied mainly on *in vitro* immortalized mammary epithelial or breast cancer-derived cell lines [36,37] that often lack luminal markers and do not reflect the morphogenetic aspects of invasion [38–40]. Presumably, one reason for the lack of luminal cell-based models is that maintaining viable and actively dividing luminal cells in culture has been an ever-present challenge.

Expanding on previous developments of *in vitro* culture [41], we set out to revisit the invasive capacity of primary human LP cells in a collagen type I matrix. To this end, we developed 3D culture conditions in which single LP cells give rise to a multicellular branched ductal network resembling the morphology of low-grade NST without requiring any genetic perturbation to do

so. Thereby, we discovered that LP cells that are taken out of their normal tissue context can actively invade via matrix remodeling. Thereby, invasive branching morphogenesis was guided by leader cells and depended on inhibition of the Rho-ROCK-myosin II signaling cascade. Finally, we observed that CRISPR-Cas9 mediated deletion of E-cadherin in normal luminal cells resulted in diffusely invading organoids resembling ILC morphology. Together, our data show that invasive branching morphogenesis resulting in low-grade NST morphology can be triggered within normal LP cells *in vitro* by specific growth conditions.

Materials and methods

Isolation and culture of human mammary epithelial cells

Healthy mammary gland tissue was processed as described previously [33,42]. In brief, reduction mamoplasty tissue was minced with scalpels into 2–3 mm³ pieces. Tissue was digested with collagenase I (Sigma-Aldrich, St Louis, MO, USA), hyaluronidase (Sigma-Aldrich), and insulin (Sigma-Aldrich) and treated with trypsin–EDTA (Invitrogen, Carlsbad, CA, USA) to create single-cell suspensions. The age and parity of donors used in this study are catalogued in supplementary material, Table S1. Cells were grown in an incubator (Thermo Fisher Scientific, Waltham, MA, USA) at 37 °C with 5% CO₂. O₂ levels were maintained at 3%.

3D culture

3D collagen type I gels were prepared as described previously [33,42] with minor modifications. Single-cell suspensions were mixed with branched luminal organoid medium (BLOM) foundation, rat tail collagen type I (Corning, Corning, NY, USA) and neutralizing solution. The final collagen concentration was 1.3 mg/ml. Upon polymerization and medium addition, gels were detached. For Matrigel experiments, LPs in a BLOM suspension were mixed with growth factor reduced Matrigel (Corning).

Inhibitor treatment

Collagen degradation via matrix metalloproteinases (MMPs) was inhibited by using 10 μM marimastat (Sigma-Aldrich), which was added to the medium of elongating organoids prior to imaging. E-cadherin blocking was performed by addition of an E-cadherin blocking antibody HECD-1 (Abcam, Cambridge, UK) at a dilution of 1:25 after 5 days of organoid culture. Para-amino blebbistatin (PAB) treatment was performed by adding 10 μM PAB (Cayman Chemical, Ann Arbor, MI, USA) to the culture medium.

CRISPR-Cas9-mediated gene knockout

Freshly sorted LP cells were expanded in 2D and subsequently transfected with the TransIT-X2 transfection reagent (Mirus Bio, Madison, WI, USA) according to the manufacturer's recommendation. Cas9-GFP-expressing plasmid (pSpCas9(BB)-2A-GFP) and the gRNA-containing STAgR_Neo plasmid were co-transfected. Fluorescence activated cell sorting (FACS) was used to enrich for modified cells. CRISPR/Cas9-induced deletions at the targeted locus were assessed from genomic DNA. To assess editing efficiency on the protein level, gels were stained for E-cadherin and structures with and without E-cadherin were quantified.

Supplementary materials and methods include details of the following: isolation and culture of human mammary epithelial cells, FACS, 3D culture, measurement of structure dimension and assessment of complexity, extreme limiting dilution analysis (ELDA), carmine staining, immunofluorescence, live-cell imaging, collagen labeling and imaging, data analysis, collagen coating and 2D culture of LP cells, CRISPR-Cas9-mediated gene knockout (KO), immunohistochemistry on tissue sections, and statistical analysis.

Results

Human mammary LP cells give rise to complex branched ductal structures in collagen type I gels

In order to recapitulate luminal cell invasion *in vitro*, we isolated LP cells from esthetic reduction mammoplasties performed on healthy donors (Figure 1A) using FACS and the established markers CD49f and EpCAM [43] (Figure 1B, supplementary material, Figure S1A). We ensured sample purity by re-analyzing sorted populations (supplementary material, Figure S1B) and only sorts with a purity of at least 99.5% were used for further experiments. As an ECM surrogate, we employed freely floating hydrogels composed of collagen type I, as described previously [33,44].

To maintain luminal cell characteristics and to ensure robust rates of proliferation, we used the breast cancer organoid medium (BCOM) as described by Sachs *et al* [41]. BCOM was previously used for culturing mammary epithelial fragments in Matrigel, thereby supporting the maintenance of the luminal as well as the basal cellular subset. We observed that in combination with collagen type I matrix, a fraction of single LP cells (CD49f^{high}/EpCAM^{high}) cultured in BCOM formed small cell clusters and gave rise to simple branched organoids with short ducts and at least two branching points (see supplementary material, Figure S1C,D). Small amounts of FCS have previously been used to increase initial survival and promote outgrowth of single primary mammary epithelial cells in culture [33]. Accordingly, we could achieve a 12-fold increase in branched structure formation of single LP cells by the addition of 0.5% FCS to the medium (see supplementary material,

Table S2), which was hereafter termed BLOM. Other morphologic shapes that occurred in both media were sticks and spheres (Figure 1C,D, supplementary material, Figure S1C,D). Notably, when cells were cultured in Matrigel instead of collagen type I, no branched structure formation occurred (see supplementary material, Figure S1E). Importantly, branched structure forming ability in collagen type I gels was not donor-specific: branched luminal organoids could be generated successfully from all donors tested ($n = 12$; Figure 1E, supplementary material, Table S1). In line with previous observations, sorted single luminal mature cells (CD49f^{low}/EpCAM^{high}) barely proliferated when cultured in BLOM in collagen type I gels, whereas single basal cells (CD49f^{high}/EpCAM^{low}/CD10⁺) also generated branched structures (see supplementary material, Figure S1F).

In summary, these data show that normal primary LP cells in collagen type I matrix have the capacity to give rise to complex branched ductal structures resembling the branched ductal morphology of low-grade NST carcinomas (Figure 1F).

Branched luminal organoids arise clonally and express luminal lineage and polarization markers

We set out to further characterize LP-derived branched structures derived in BLOM, focusing on frequency, morphogenetic steps, and lineage marker expression. First, we performed ELDA to calculate the proportion of cells within the LP population that have structure-forming potential [45]. For this purpose, sorted LP cells were seeded in limiting dilution into collagen type I gels and their single-cell state was confirmed by light microscopy, thus confirming that arising structures were of clonal origin. Thereby, we determined that overall, one of 15 freshly sorted LP cells had the capacity to grow into a branched ductal structure (Table 1). Through low seeding density and daily microscopic analysis, we ruled out that branched structures at a later stage resulted from merged organoids. Moreover, monitoring of organoid growth revealed different growth phases. During the establishment phase (days 1–5), single LP cells started proliferating and formed small cell clusters. Around day 5 of culture, small ducts were formed, which further expanded into the matrix, whereby structure complexity continuously increased (elongation/branching phase, days 5–10). Finally, we observed decreased duct elongation accompanied by rounding up and thickening of the tips (days 11–13) (Figure 2A).

Building on the morphologic resemblance to low-grade NST, we next set out to assess lumen formation and luminal marker expression as hallmarks of low-grade NST pathology (Figure 2B). Those markers include CK8/18 [46], GATA3 [11,12], ZO-1 [47], and mucin-1 [48]. Confocal immunofluorescence of fully grown organoids (days 11–13) revealed expression of intermediate filaments CK8/18 within the cytoplasm (Figure 2C) and nuclear expression of transcription factor GATA3 (Figure 2D) in all organoids examined.

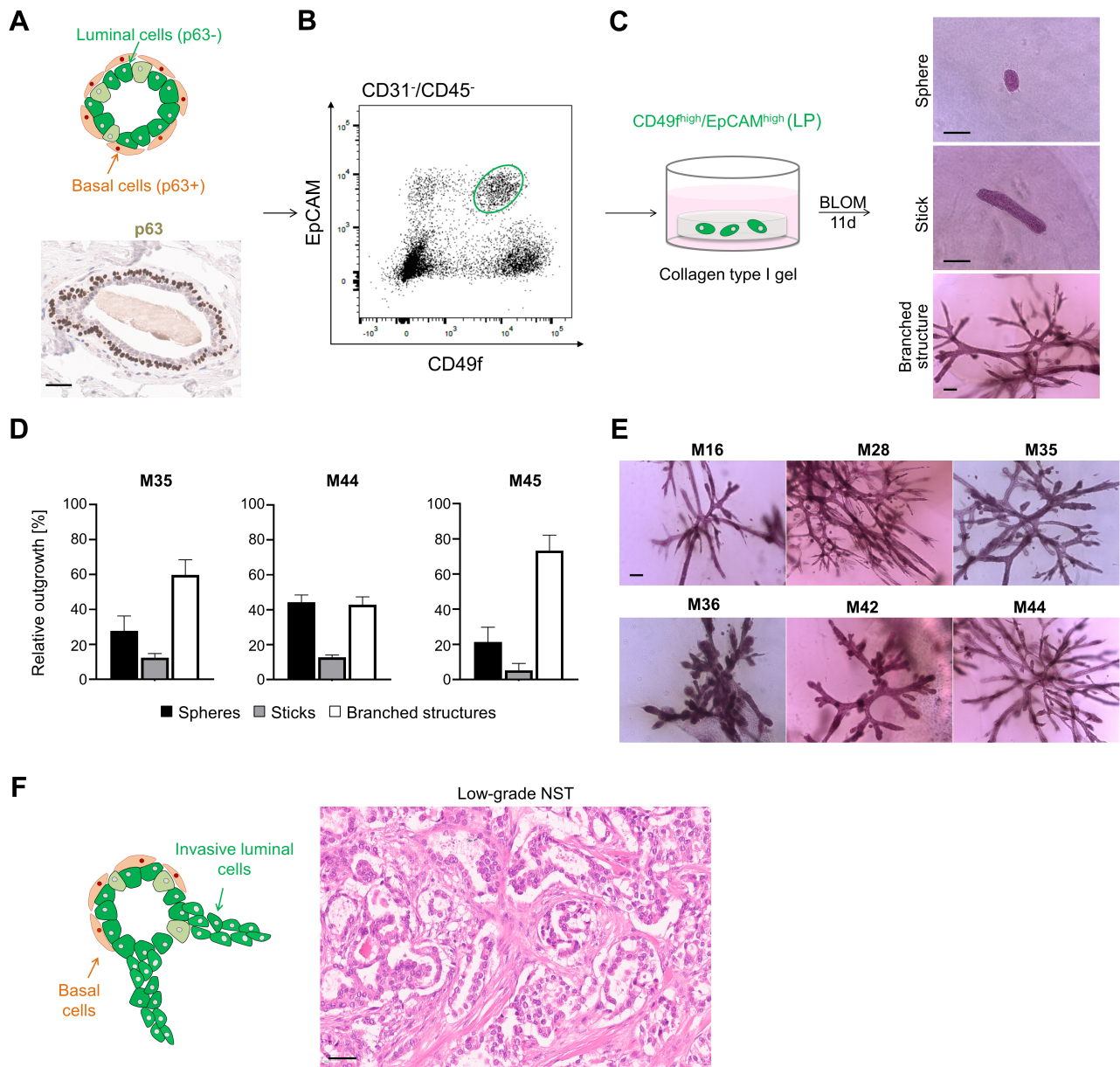


Figure 1. Human mammary LP cells give rise to complex branched ductal structures in collagen type I gels. (A) Normal mammary gland morphology: schematic illustration and p63-stained section (brown) of normal mammary duct. Scale bar: 50 μ m. (B) Sorting of epithelial cells from reduction mammoplasties via FACS based on EpCAM and CD49f expression. The green circle indicates the CD49f^{high}/EpCAM^{high} population (= LP). (C) Experimental set-up with carmine staining of arising structure types in BLOM. Scale bar: 100 μ m. (D) Quantification of outgrowing structure types in BLOM. Depicted are donors M35, M44, and M45. Structure type was normalized to total structures arising per gel. Data are mean \pm SD, $n = 4$ gels/condition. (E) Carmine staining of branched structures arising from donors M16, M28, M35, M36, M42, and M44 in BLOM. Scale bar: 100 μ m. (F) Schematic illustration of invasively growing LP cells and section of low-grade NST carcinoma. Scale bar: 50 μ m.

Throughout the organoids, we observed a non-continuous lumen mostly framed by a single-cell layer (Figure 2C–H). Previously, correct apical-basal polarization of the epithelium has been shown to be a prerequisite for lumen formation during collective invasion of epithelial cells [49]. In line with these notions, we detected expression of tight junction protein ZO-1 at an apical position of the ducts, indicating correct apical-basal polarization in all organoids examined (Figure 2E,I). Supporting the same notion, we discovered mucin-1, a marker of luminal differentiation, expressed at the apical side (Figure 2F,I). To corroborate

this observation, we examined the non-lineage specific polarization markers laminin and F-actin within individual ducts. We observed that the basolateral side of most ducts was covered by the basal lamina component laminin (Figure 2G,I), whereas an accumulation of F-actin towards the apical side was found at locations where a lumen was formed (Figure 2H,I). In addition, we investigated the expression of basal lineage markers p63 and alpha smooth muscle actin (α -SMA) [38], which are typically absent in NSTs (Figure 2B). We used basal cell-derived organoids as a positive control, which reliably expressed p63 and α -SMA (see supplementary material,

Table 1. ELDA: determination of branched structure-forming units (B-SFU).

Number of cells seeded	Positive gels/total gels		
	M36	M44	M50
5	1/6	3/6	N/A
10	2/6	4/6	2/6
20	5/6	5/6	4/6
40	6/6	6/6	5/6
80	6/6	6/6	6/6
160	6/6	6/6	6/6
320	N/A	N/A	6/6
B-SFU	1/15.1	1/9.52	1/20.7
95% CI	1/8.85–1/26	1/5.53–1/16.7	1/11.8–1/36.5
Mean B-SFU		1/15.11	

N/A, not available.

Figure S2A,C). In contrast, neither p63 nor α -SMA was detected within luminal organoids (see supplementary material, Figure S2B,D).

In summary, these results show, for the first time, that upon transplantation into a collagen type I environment, a large fraction of normal primary LP cells bears the potential of growing out into clonal, complex branched structures. Doing so, luminal cells maintained their lineage marker expression and mature ducts displayed apical-basal polarity as well as lumen formation. As a result, mature organoids resemble low-grade NST in morphology and lineage marker expression.

LP-derived branched organoid formation requires inhibition of ROCK-myosin II signaling

In contrast to previous experimental set-ups, where LP cells cultured in collagen type I gels gave rise to small spheres [33,50], we observed the formation of highly polarized, branched structures. Importantly, it has been shown that invasion as well as apical-basal polarization of epithelial structures in collagen type I matrices requires regulation of RhoA-ROCK-myosin II signaling via inhibition of the Rho-associated protein kinase (ROCK) [51,52]. Thus, we speculated, that the ROCK inhibitor Y-27632, which is a constant component of the BLOM medium, but has not been added continuously in previous studies, might play a critical role for branched structure formation and polarization of LP-derived organoids. Indeed, in medium devoid of Y-27632, the formation of elongated branched structures was almost completely prevented (Figure 3A). In detail, the removal of Y-27632 led to a decrease in branched structure formation by 79%. Instead, most cells grew out as spheres and sticks (Figure 3B, supplementary material, Figure S3A). Furthermore, the rarely emerging branched structures were significantly smaller in size (–66%) (Figure 3C) and showed a reduced branching complexity. Specifically, only 6% of organoids showed tertiary or even more complex branches, in contrast to

65% of control organoids (see supplementary material, Figure S3B).

In addition, immunofluorescence revealed that polarization was disturbed in the absence of ROCK inhibition (Figure 3D). Specifically, LP structures derived in the absence of Y-27632 lacked lumen formation, and neither laminin deposition at the basolateral side nor F-actin accumulation at the apical side was observed. Finally, we set out to provide further support for inhibition of the ROCK-myosin II pathway as a prerequisite for branched structure formation by targeting a different segment of this pathway. To do so, we replaced Y-27632 by PAB, an inhibitor of the ROCK downstream target myosin II. Indeed, PAB was able to induce a phenotype similar to the one created by Y-27632 (see supplementary material, Figure S3C,D).

Next, we wanted to assess the dynamics of the process required for the formation of LP-derived branched structures and its dependency on ROCK inhibition. For this purpose, we performed live-cell confocal microscopy during the organoid elongation phase, focusing on the cellular dynamics within branched organoids and their interaction with the surrounding collagen matrix. Specifically, we monitored cellular movements within LP-derived branched organoids in the presence and absence of Y-27632 using nuclear labeling. Thereby, we observed that under ROCK inhibition, cell migration was primarily directed outwards in parallel to the axis of the extending duct. This directionality was significantly diminished in conditions without ROCK inhibitor. Here, the parallel (V_{II}) and orthogonal (V_I) velocities were more similar, resulting in a less directed movement (Figure 3E). Furthermore, to visualize cellular interaction of the cells with the surrounding ECM, we conducted live-cell imaging of organoids in collagen type I gels spiked with fluorescent tracer particles/beads. Doing so, we observed that in the presence of ROCK inhibitor, bead displacement and, therefore, contractility was not completely abolished but limited to the front of elongating ducts (Figure 3F, supplementary material, Movie S1). By contrast, in the absence of ROCK inhibition we observed strong, generalized bead displacement towards the organoids, suggesting high cellular contractility (Figure 3G, supplementary material, Movie S2).

Together, these results show that in normal LP cells, reduction of the ROCK-myosin II signaling enables directed contractility and migration, resulting in branching morphogenesis and concomitant apical-basal polarization in collagen type I gels.

Ductal organoids are generated through invasive branching morphogenesis

As previously described, active cellular invasion is facilitated by remodeling of the ECM [53]. Importantly, the above-described engagement with the ECM was suggestive of matrix remodeling as a driver of luminal organoid formation. Therefore, we hypothesized that in order to undergo branching morphogenesis resulting in the

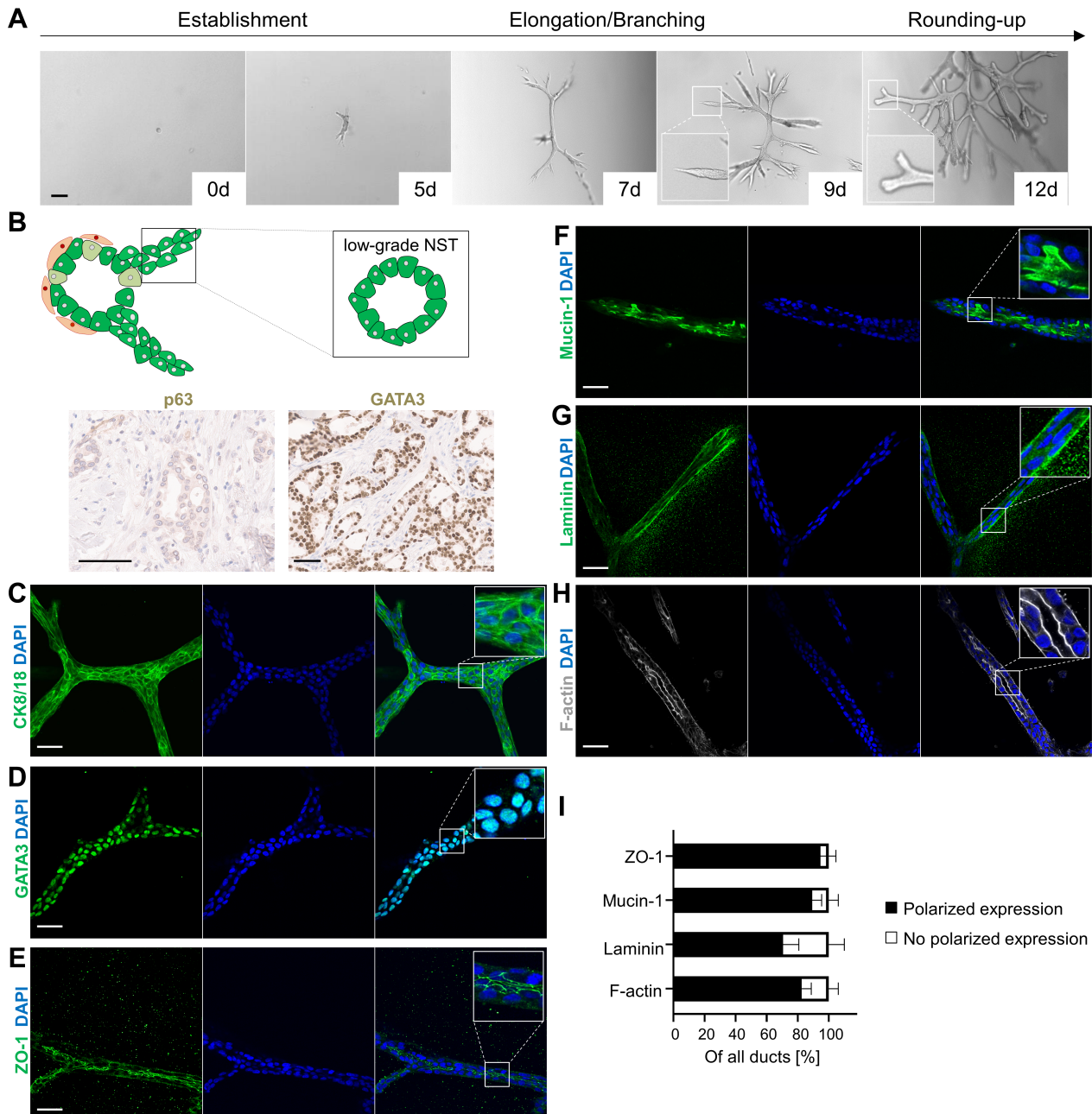


Figure 2. Branched luminal organoids arise clonally and express luminal lineage and polarization markers. (A) Light microscopy pictures of a branched luminal organoid developing from a single cell over the course of 12 days. Scale bar: 100 μ m. (B) Schematic illustration of invasively growing LP cells and p63 (brown) or GATA3 (brown) stained section of ducts arising in low-grade NST carcinomas. Scale bar: 50 μ m. (C–H) Confocal microscopy on branched LP-derived organoids: representative images of luminal and polarization markers. Organoids were stained for CK8/18 (green), GATA3 (green), ZO-1 (green), mucin-1 (green), laminin (green), F-actin (white), and DAPI (blue). $n = 30$ structures/condition; 3 donors; 10 structures/donor. Scale bar: 50 μ m. (I) Quantification of ducts with and without correctly polarized expression of markers. Data are presented as stacked bars with mean \pm SD, $n = 25$ ducts.

observed low-grade morphology of NST carcinoma, LP cells need to invade the ECM actively and collectively. To address this, we first focused on matrix topography to understand invasive mechanisms exploited by LP cells.

Normal mammary epithelium is typically surrounded by curly, anisotropic collagen fibers [54]. Upon tumor initiation, collagen fibers are linearized, which promotes migration and invasion of breast cancer cells along aligned fibers. This alignment has been shown to be

facilitated by invading carcinoma cells [54,55]. Similarly, using fluorescently labeled collagen type I, we observed an alignment of collagen fibers in front of the extending ducts. By contrast, collagen fibers in the periphery of the organoid showed no preferred orientation (Figure 4A, supplementary material, Figure S4A). Importantly, it is well known that fiber alignment requires ROCK-mediated cellular contractility [55,56]. This further supports the notion that ROCK inhibition as used in our model does not completely abolish cellular contractility,

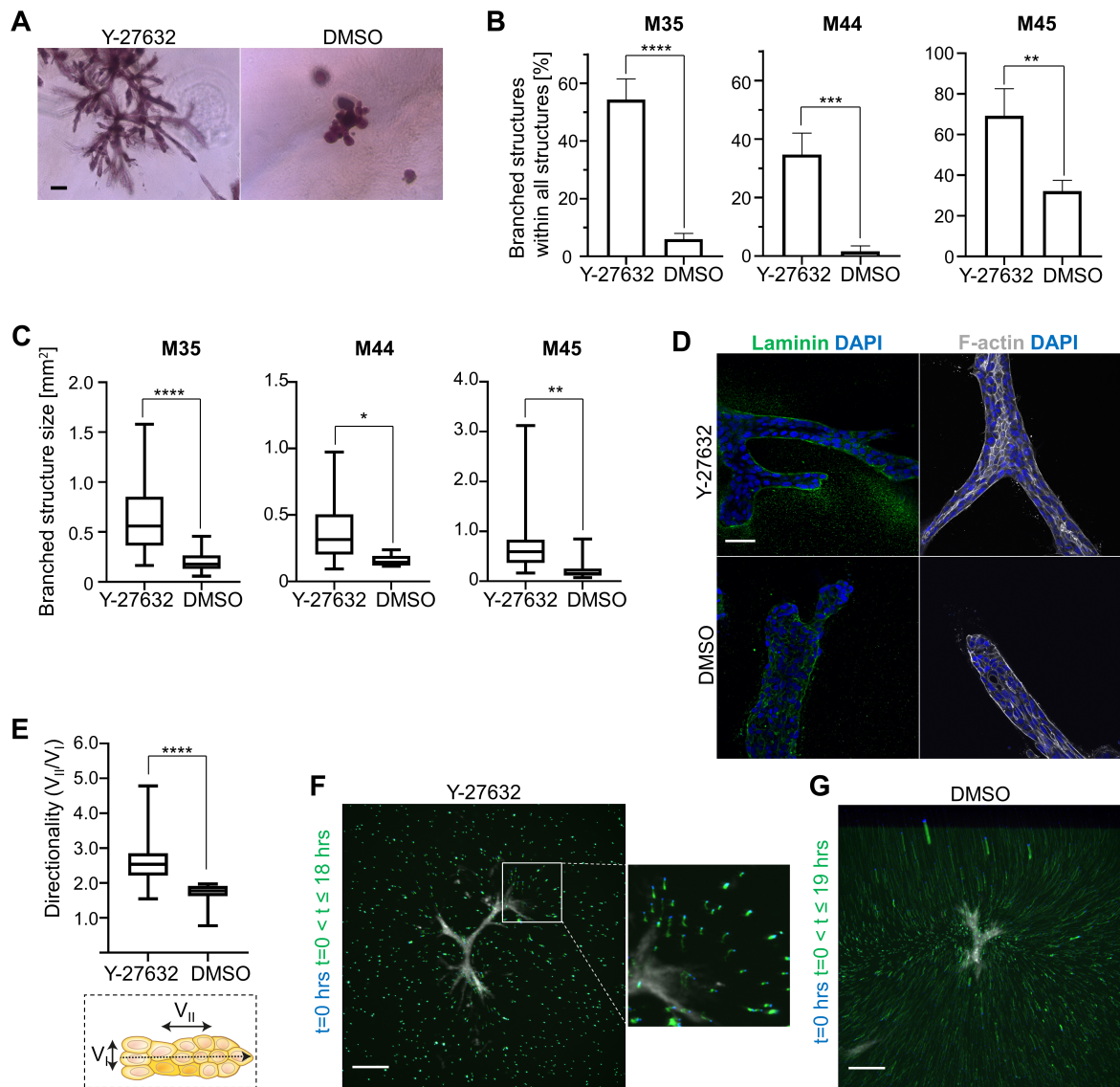


Figure 3. LP-derived branched organoid formation requires inhibition of ROCK-myosin II signaling. (A) Carmine staining of branched structures arising in BLOM with Y-27632 or without (DMSO control). Scale bar: 100 μ m. (B) Quantification of branched structures in BLOM with Y-27632 or without (DMSO control). Depicted are donors M35, M44, and M45. Branched structures were normalized to total structures arising per gel. Data are mean \pm SD, $n = 4$ gels/condition. P values were calculated using an unpaired two-tailed t -test, ** $p \leq 0.01$, *** $p \leq 0.001$, **** $p \leq 0.0001$. (C) Quantification of branched structure sizes in BLOM with Y-27632 or without (DMSO control). Depicted are donors M35, M44, and M45. Size was defined as the area covered by the organoid when all tips were connected virtually using ImageJ. Data are shown as median \pm 25%. $n = 4$ gels/condition. P values were calculated using an unpaired two-tailed t -test, * $p \leq 0.05$, ** $p \leq 0.01$, **** $p \leq 0.0001$. (D) Confocal microscopy of branched luminal organoids grown in BLOM with Y-27632 or without (DMSO control): representative images of polarization markers. Organoids were stained for laminin (green), F-actin (white), and DAPI (blue). Scale bar: 50 μ m. (E) Top: directionality of cellular movement calculated as quotient of velocity directed in parallel to extending duct (V_{II}) and orthogonal to it (V_I). Data are shown as median \pm 25%. P value was calculated using an unpaired two-tailed t -test, **** $p \leq 0.0001$. Bottom: schematic depiction of elongating duct. (F,G) Displacement of fluorescent beads relative to $t = 0$ measured by live-cell imaging with Y-27632 or without (DMSO control). $t = 0$ h (blue) versus $t = 0 < t \leq 18/19$ h (green). Scale bar: 200 μ m. Experiments were repeated in $n = 3$ donors with a total of individual organoids $n \geq 30$.

but rather reduces it to a level enabling directed movement of cells as well as rearrangement of collagen fibers. Another crucial aspect of matrix remodeling during invasion is active degradation by MMPs, which has also been observed as a competence of epithelial cells during cancer cell invasion [57–59]. Accordingly, live-cell imaging revealed that treatment with the MMP inhibitor marimastat during the duct elongation phase stopped the duct tips from further invading the matrix. At the same time, cell movements

and divisions persisted within the organoid body, thereby excluding a general cytotoxic effect of marimastat treatment (Figure 4B, supplementary material, Figure S4B, Movies S3, S4). Of note, we found that during the observed elongation phase, the distinct expression of laminin as described for fully grown organoids was not established yet. This finding helps to explain how direct interaction of the invading cells with the collagenous ECM is enabled (see supplementary material, Figure S4C,D).

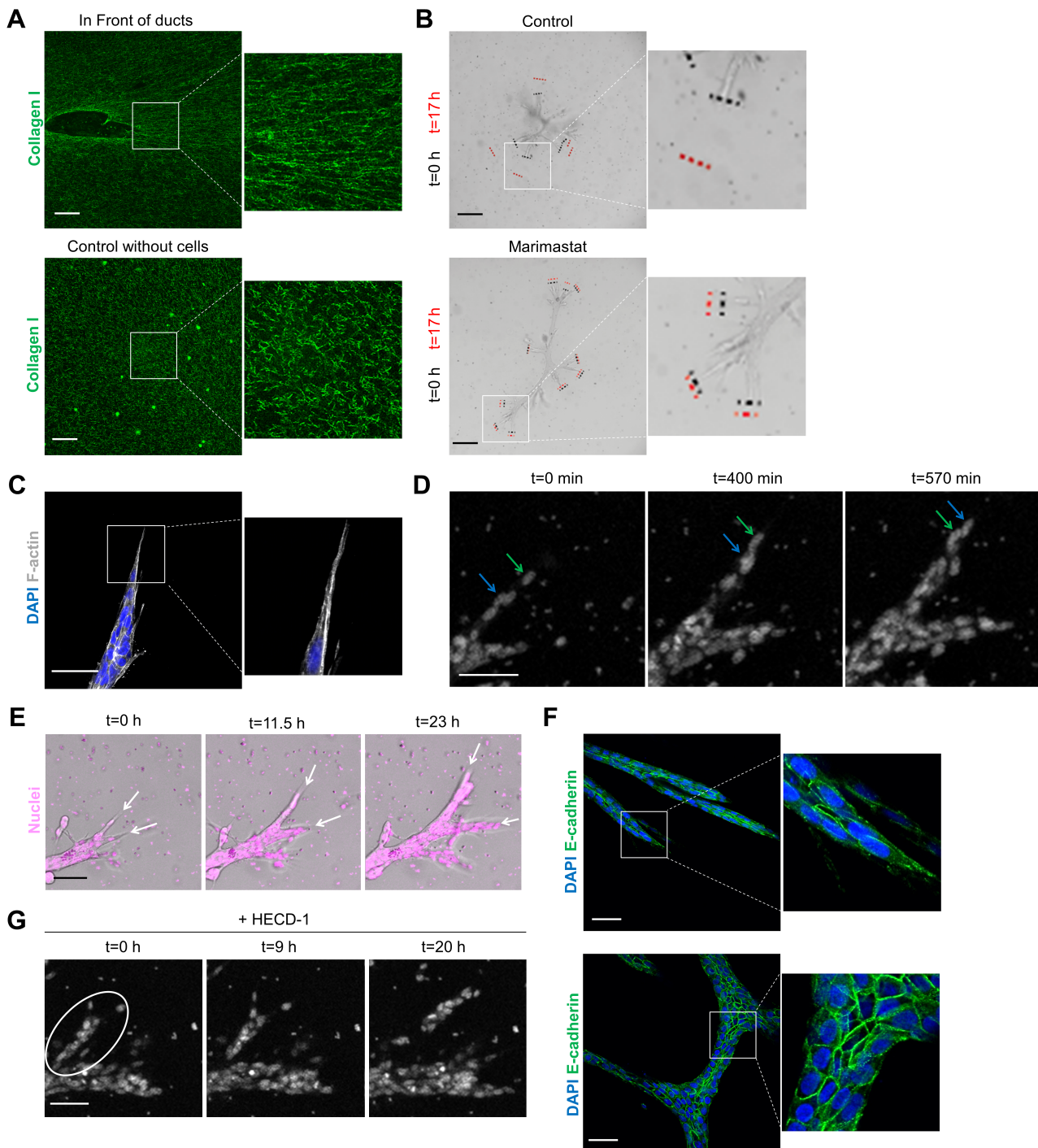


Figure 4. Ductal organoids are generated through invasive branching morphogenesis. (A) Alignment of collagen fibers in front of invading ducts versus in control sections of the gel without cells. Scale bar: 50 μm . $n = 22$ individual organoids. (B) Duct elongation upon treatment with marimastat versus untreated control organoids measured by live-cell imaging with $t = 0$ h (black) versus $t = 17$ h (red). Scale bar: 200 μm . $n = 18$ individual organoids. (C) Confocal microscopy on tip cell stained for F-actin (white) and DAPI (blue). Scale bar: 50 μm . (D) Tip cell exchange. Cells tracked by live-cell imaging. Tip cell 1 (green arrow), tip cell 2 (blue arrow). Organoids measured by live-cell imaging via nuclear labeling with sirDNA (white). Scale bar: 50 μm . (E) Bifurcation at tip. Organoids measured by live-cell imaging via nuclear labeling with sirDNA (pink). Scale bar: 80 μm . (F) Confocal microscopy on invading organoid stained for E-cadherin (green) and DAPI (blue). Scale bar: 50 μm . (G) Duct elongation of organoid (day 8) upon addition of HECD-1 antibody on day 5. Organoids measured by live-cell imaging over the course of 20 h via nuclear labeling with sirDNA (white). Scale bar: 50 μm . $n = 30$ individual organoids.

In addition, invasive branching morphogenesis is characterized by the formation of an invasive front guided by a leader cell [60]. Accordingly, we found that during the elongation phase, a single cell was observed at the tip of each duct which exhibited an extended

morphology characterized by filopodia-like membrane protrusions (Figure 4C). Matching this observation, live-cell imaging revealed that during the elongation phase, one cell was situated at the tip of each continuously outgrowing duct and remained at this front

position over several hours (see supplementary material, Figure S4E, Movie S5). However, we also observed that the leader cell was not *per se* specialized, but could be

exchanged by a cell from the structure body (Figure 4D, supplementary material, Movie S6). Moreover, if two neighboring leader cells with differentially

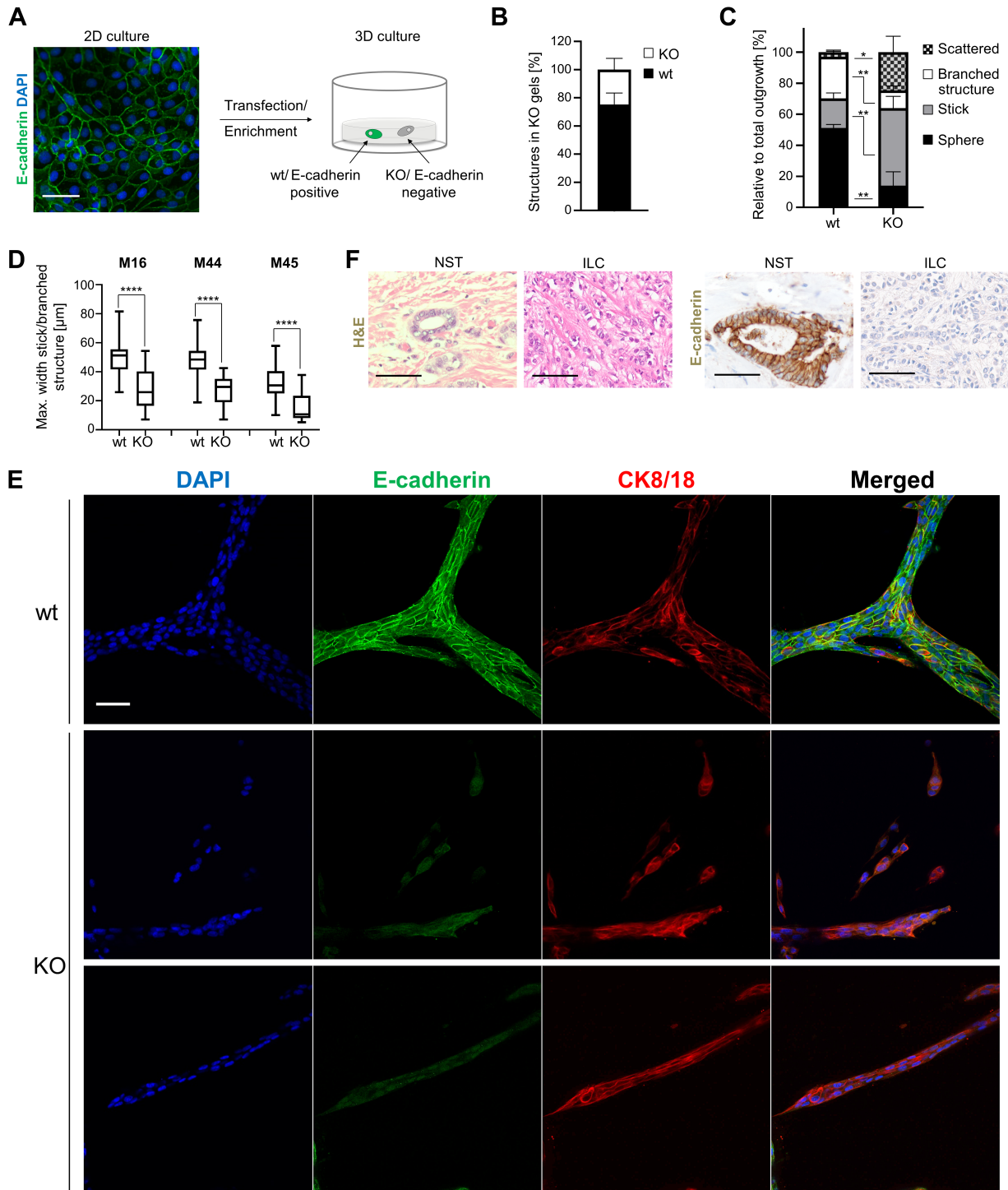


Figure 5. Deletion of E-cadherin results in ILC-like morphology. (A) Immunofluorescence of E-cadherin expression in 2D culture and schematic illustration of clonal outgrowth in 3D culture upon transfection and enrichment. Cells were stained for E-cadherin (green) and DAPI (blue). Scale bar: 50 μ m. (B) Modification efficiency on the protein level. All structures found in gels after transfection and enrichment were classified via confocal microscopy by E-cadherin status into wt versus KO structures. Data are presented as stacked bar with mean \pm SD of $n = 3$ donors. (C) Quantification of structure type arising in collagen gels after transfection and enrichment divided by E-cadherin status of the structures (wt versus KO). Each structure category was normalized to the total number of structures per condition. Data are presented as stacked bar with mean \pm SD of $n = 3$ donors. (D) Quantification of maximum width of arising branched structures and sticks. Structures are divided by E-cadherin status into wt versus KO. Data are shown as median \pm 25%. P values were calculated using an unpaired two-tailed t -test, **** $p \leq 0.0001$. (E) Confocal microscopy on structures growing out in collagen gels after transfection and enrichment that either still maintained E-cadherin (wt) or had lost it (KO). Structures were stained for E-cadherin (green), CK8/18 (red), and DAPI (blue) Scale bar: 50 μ m. (F) H&E and E-cadherin (brown) stained section of NST carcinoma and ILC. Scale bar: 50 μ m.

oriented filopodia-like protrusions were present, the ducts bifurcated, thereby increasing the complexity of the structure (Figure 4E and supplementary material, Movie S7).

Transfer of leader cell-generated forces along epithelial cohorts during collective invasion has been described to depend on cadherin-mediated cell–cell junctions [61]. Immunofluorescence confirmed that cells in invading structures were tightly connected with the leader cell and with each other via expression of E-cadherin (Figure 4F). Based on these considerations, the importance of E-cadherin-mediated cell–cell junctions during collective invasion was determined by treating structures with a function blocking antibody (HECD-1). Live-cell imaging of HECD-1-treated organoids during the elongation phase revealed dissolution of invasive branching morphogenesis with single cells or even whole ducts losing contact to the structure body (Figure 4G, supplementary material, Movie S8). Consequently, we saw scattering of the cells with subsequent loss of duct coherence (see supplementary material, Figure S4F).

Together, these results show that normal LP cells actively invade into the ECM via matrix remodeling. Thereby, interchangeable leader cells guide invasive branching morphogenesis. Finally, tight cell–cell connections with the leader cell, mediated, at least in part by E-cadherin, ensure duct integrity during collective invasion.

Deletion of E-cadherin results in ILC-like morphology

The strong impact on organoid morphology observed upon E-cadherin inhibition is in line with the critical role of E-cadherin status in invasive cancer formation. Indeed, E-cadherin status is the main discriminator between NST and ILC, a specific, morphologically distinct subtype of invasive cancer. Whereas NSTs typically express high levels of E-cadherin, in ILC, full loss of genetic function and therefore protein expression is typically observed [14,15].

Based on these considerations, we set out to recapitulate the full deletion of E-cadherin encoded by *CDH1* with the CRISPR-Cas9 system. Doing so, we wanted to take advantage of the clonality of outgrowing organoids to create clonal KO structures. To efficiently perform the KO, we tested whether organoid-forming potential of LP cells was maintained during prior 2D culture, which greatly facilitated efficient transfection and expansion in contrast to 3D culture. Indeed, we determined that 3D branched ductal organoids could be generated even after three passages in standard 2D culture (see supplementary material, Figure S5A).

After transfection of LP cells in 2D and enrichment for successfully transfected cells via a GFP-tagged Cas9 plasmid using FACS, single LP cells were seeded into collagen type I gels (Figure 5A). Upon KO with two gRNAs framing a section of exon 5, we saw a partial deletion at the genetic level within the sorted population (see supplementary material, Figure S5B,C). Due to the

clonal growth of single cells within the assay, we were able to differentiate between wildtype (wt) and KO organoids by E-cadherin immunofluorescence. Overall, we observed a mixture of wt and KO organoids with around 25% of organoids bearing the KO (Figure 5B). Notably, in control gels with empty-vector transfected cells, no E-cadherin-negative structures were observed (data not shown). Importantly, the phenotypes of fully grown wt and KO structures were strikingly different. Wt cells grew into sticks, spheres, and complex branched structures displaying the previously described morphology. In contrast, the ducts of KO organoids were typically thinner, and they often showed stick-like instead of branched morphology. Several KO structures showed partial loss of cell–cell contact and were scattered throughout the gel or forming single rows of invading cells. In addition, a decrease in sphere formation was observed (Figure 5C–E). To exclude that the aberrant morphology was the result of loss of proliferative capacity, we performed a Ki67 staining and determined that KO and wt structures showed similar rates of proliferation (see supplementary material, Figure S5D,E).

Taken together, the morphology we observed upon KO of E-cadherin was reminiscent of the growth pattern that ILCs exhibit *in vivo*, which is characterized by the absence of duct formation and cells penetrating the matrix as single cells or thin files of cells (Figure 5F) [62]. Thus, we conclude that KO of a gene relevant for invasive branching morphogenesis has an impact on the resulting phenotype in our model that is comparable with its effect in patients *in vivo*.

Discussion

When cultured in collagen type I gels under defined conditions, up to 10% of freshly isolated normal LP cells generated complex multicellular organoids through invasive branching morphogenesis. Considering that tissue isolation and FACS prior to 3D culture can drastically reduce the viability of primary LP cells, we hypothesize that matrix invasion potential does not represent the ability of a rare luminal subset. Rather, our results indicate that almost every single LP cell bears matrix invasion potential that can be triggered under suitable conditions. This supports the theory that invasion potential is already existent in pre-invasive malignancies rather than being unlocked in the luminal compartment as a consequence of specific genetic aberrations [16–20].

Morphologically, the organoids arising from unmodified LPs resemble low-grade NST by phenocopying branching morphogenesis or, said differently tubulogenesis, which represents an important parameter for assigning tumor grade. The resulting low-grade phenotype is in line with the correlation of mutational load and tumor grade as described previously [63].

Even though invasive behavior *per se* has not been connected to specific genetic aberrations in the luminal

population, certain perturbations impact invasive branching morphogenesis and are strongly associated with breast cancer subtype. Our single-cell-based assay allows insertion and precise quantification of phenotypes connected to genetic aberrations, as shown by the analysis of an E-cadherin KO phenotype. Here, the KO morphology mirrors the loss of duct formation and thereby closely resembles clinical samples of the ILC subtype. Therefore, the experimental system presented here is a useful tool for unraveling the gene-specific impact on invasive subtype and screening purposes based on phenotype.

Despite relying on direct contact to collagen type I, matrix invasion of LP cells was highly dependent on ROCK inhibition. This suggests that an activation of the ROCK-myosin II signaling cascade represents an invasion-suppressing response of LP cells upon contact to the collagenous ECM. A similar observation has been reported recently for murine cells *in vivo*, where it was shown that the mere contact to the ECM did not result in luminal cell invasion. However, invasion was enabled once the functionality of actomyosin contractility regulator MYPT1 was reduced within the luminal cells [64]. This phenomenon has further been reported in *in vitro* studies with immortalized normal-like mammary epithelial cells [32] as well as epithelial kidney cells [51]. In both cases, ROCK inhibition enabled cellular invasion into a collagen type I matrix. In our model, we observed residual contractility even upon ROCK inhibition as indicated by spatially restricted bead displacement and collagen fiber alignment, which in turn further supports directional migration [54,56]. In line with these considerations, Schipper *et al* [64] showed that a full obstruction of MYPT1 function resulted in a loss of invasive capacity *in vivo*. Together, these results highlight the importance of a tightly balanced actomyosin contractility for luminal cell invasion rather than a full obstruction.

The ECM invasion process is based on complex interactions between epithelial and stromal cells and the surrounding matrix. Stromal cells, particularly cancer-associated fibroblasts, have been described as matrix remodeling drivers of invasion [53,65,66]. Our work puts the spotlight exclusively on the interaction of luminal cells with the surrounding collagen matrix, which *in vivo* only occurs once the basal cell layer and basement membrane barrier are disrupted. Nevertheless, our work shows that once the contact between LP cells and collagen type I is established, luminal cells can actively invade without the requirement for genetic aberrations or stromal support.

In our model, reduced contractility is required for invasive branching morphogenesis of luminal cells, yet we lack detailed understanding of how the same mechanism could be utilized *in vivo* during invasion of malignant luminal cells. The inability to identify universal aberrations between invasive and *in situ* carcinomas might hint towards participation of stromal factors for the reduction of actomyosin contractility. Future studies in which the collagen gels are complemented with

cancer-associated stromal cells will help to elucidate the relevance of stromal interactions during luminal cell invasion. Thus, by furthering our knowledge on luminal cell invasion, this model will help us to find new means for early diagnosis and prevention of invasive cancers arising from the LP subset.

Acknowledgements

We are grateful for feedback and support from the Khaled group (Department of Pharmacology, University of Cambridge), particularly Walid Khaled and Alecia-Jane Twigger. We thank Heiko Lickert (Institute of Diabetes and Regeneration Research, Helmholtz Center Munich), Stefan Stricker (Institute for Stem Cell Research, ISF, Helmholtz Center Munich), and Magdalena Götz (Institute for Stem Cell Research, Helmholtz Center Munich) for helpful discussions. We further acknowledge the support from all members of the Scheel group for their encouragement and sharing scientific expertise. This work was supported by grants from the German Cancer Aid foundation (Max Eder Program, Deutsche Krebshilfe, #110225 to CHS and Integrate-TN, Deutsche Krebshilfe, #70113450 to WW).

Author contributions statement

HMG, LKE and CHS conceived the project. HMG, LKE, BB and LE designed and conducted experiments. HMG, LKE and CG processed reduction mammoplasties. MJ, GS and AM performed immunohistochemistry. Data were interpreted by HMG, LKE, BB, CHS and ARB. The manuscript was prepared by HMG, LKE, BB and CHS and critically reviewed by all authors.

References

1. Molyneux G, Geyer FC, Magnay FA, *et al*. BRCA1 basal-like breast cancers originate from luminal epithelial progenitors and not from basal stem cells. *Cell Stem Cell* 2010; **7**: 403–417.
2. Tao L, van Bragt MPA, Li Z. A long-lived luminal subpopulation enriched with alveolar progenitors serves as cellular origin of heterogeneous mammary tumors. *Stem Cell Reports* 2015; **5**: 60–74.
3. Proia TA, Keller PJ, Gupta PB, *et al*. Genetic predisposition directs breast cancer phenotype by dictating progenitor cell fate. *Cell Stem Cell* 2011; **8**: 149–163.
4. Lim E, Vaillant F, Wu D, *et al*. Aberrant luminal progenitors as the candidate target population for basal tumor development in BRCA1 mutation carriers. *Nat Med* 2009; **15**: 907–913.
5. Lopez-Garcia MA, Geyer FC, Lacroix-Triki M, *et al*. Breast cancer precursors revisited: molecular features and progression pathways. *Histopathology* 2010; **57**: 171–192.
6. Li CI, Anderson BO, Daling JR, *et al*. Trends in incidence rates of invasive lobular and ductal breast carcinoma. *JAMA* 2003; **289**: 1421–1424.

7. Bloom HJ, Richardson WW. Histological grading and prognosis in breast cancer; a study of 1409 cases of which 359 have been followed for 15 years. *Br J Cancer* 1957; **11**: 359–377.
8. Contesso G, Mouriessse H, Friedman S, et al. The importance of histologic grade in long-term prognosis of breast cancer: a study of 1,010 patients, uniformly treated at the Institut Gustave-Roussy. *J Clin Oncol* 1987; **5**: 1378–1386.
9. Elston CW, Ellis IO. Pathological prognostic factors in breast cancer. I. The value of histological grade in breast cancer: experience from a large study with long-term follow-up. *Histopathology* 1991; **19**: 403–410.
10. Patey DH, Scarff RW. The position of histology in the prognosis of carcinoma of the breast. *Lancet* 1928; **1**: 801–804.
11. Guo Y, Yu P, Liu Z, et al. Prognostic and clinicopathological value of GATA binding protein 3 in breast cancer: a systematic review and meta-analysis. *PLoS One* 2017; **12**: e0174843.
12. Naylor MJ, Ormandy CJ. Gata-3 and mammary cell fate. *Breast Cancer Res* 2007; **9**: 302.
13. Taylor-Papadimitriou J, Stampfer M, Bartek J, et al. Keratin expression in human mammary epithelial cells cultured from normal and malignant tissue: relation to in vivo phenotypes and influence of medium. *J Cell Sci* 1989; **94**: 403–413.
14. Gamallo C, Palacios J, Suarez A, et al. Correlation of E-cadherin expression with differentiation grade and histological type in breast carcinoma. *Am J Pathol* 1993; **142**: 987–993.
15. Moll R, Mitze M, Frixen UH, et al. Differential loss of E-cadherin expression in infiltrating ductal and lobular breast carcinomas. *Am J Pathol* 1993; **143**: 1731–1742.
16. Ma XJ, Salunga R, Tuggle JT, et al. Gene expression profiles of human breast cancer progression. *Proc Natl Acad Sci U S A* 2003; **100**: 5974–5979.
17. Porter D, Lahti-Domenici J, Keshaviah A, et al. Molecular markers in ductal carcinoma in situ of the breast. *Mol Cancer Res* 2003; **1**: 362–375.
18. Petridis C, Brook MN, Shah V, et al. Genetic predisposition to ductal carcinoma in situ of the breast. *Breast Cancer Res* 2016; **18**: 22.
19. Martelotto LG, Baslan T, Kendall J, et al. Whole-genome single-cell copy number profiling from formalin-fixed paraffin-embedded samples. *Nat Med* 2017; **23**: 376–385.
20. Casasent AK, Schalck A, Gao R, et al. Multiclonal invasion in breast tumors identified by topographic single cell sequencing. *Cell* 2018; **172**: 205–217.e12.
21. Cowell CF, Weigelt B, Sakr RA, et al. Progression from ductal carcinoma in situ to invasive breast cancer: revisited. *Mol Oncol* 2013; **7**: 859–869.
22. Nelson CM, Bissell MJ. Of extracellular matrix, scaffolds, and signaling: tissue architecture regulates development, homeostasis, and cancer. *Annu Rev Cell Dev Biol* 2006; **22**: 287–309.
23. Hu M, Yao J, Carroll DK, et al. Regulation of in situ to invasive breast carcinoma transition. *Cancer Cell* 2008; **13**: 394–406.
24. Sirka OK, Shamir ER, Ewald AJ. Myoepithelial cells are a dynamic barrier to epithelial dissemination. *J Cell Biol* 2018; **217**: 3368–3381.
25. Barsky SH, Karlin NJ. Myoepithelial cells: autocrine and paracrine suppressors of breast cancer progression. *J Mammary Gland Biol Neoplasia* 2005; **10**: 249–260.
26. Man YG, Sang QX. The significance of focal myoepithelial cell layer disruptions in human breast tumor invasion: a paradigm shift from the “protease-centered” hypothesis. *Exp Cell Res* 2004; **301**: 103–118.
27. Gudjonsson T, Adriance MC, Sternlicht MD, et al. Myoepithelial cells: their origin and function in breast morphogenesis and neoplasia. *J Mammary Gland Biol Neoplasia* 2005; **10**: 261–272.
28. Lagacé R, Grimaud JA, Schürch W, et al. Myofibroblastic stromal reaction in carcinoma of the breast: variations of collagenous matrix and structural glycoproteins. *Virchows Arch A Pathol Anat Histopathol* 1985; **408**: 49–59.
29. Egeblad M, Rasch MG, Weaver VM. Dynamic interplay between the collagen scaffold and tumor evolution. *Curr Opin Cell Biol* 2010; **22**: 697–706.
30. Levental KR, Yu H, Kass L, et al. Matrix crosslinking forces tumor progression by enhancing integrin signaling. *Cell* 2009; **139**: 891–906.
31. Nguyen-Ngoc K-V, Cheung KJ, Brenot A, et al. ECM microenvironment regulates collective migration and local dissemination in normal and malignant mammary epithelium. *Proc Natl Acad Sci U S A* 2012; **109**: E2595–E2604.
32. Carey SP, Martin KE, Reinhart-King CA. Three-dimensional collagen matrix induces a mechanosensitive invasive epithelial phenotype. *Sci Rep* 2017; **7**: 42088.
33. Linnemann JR, Miura H, Meixner LK, et al. Quantification of regenerative potential in primary human mammary epithelial cells. *Development* 2015; **142**: 3239–3251.
34. Cheung KJ, Gabrielson E, Werb Z, et al. Collective invasion in breast cancer requires a conserved basal epithelial program. *Cell* 2013; **155**: 1639–1651.
35. Gudjonsson T, Rønnev-Jessen L, Villadsen R, et al. Normal and tumor-derived myoepithelial cells differ in their ability to interact with luminal breast epithelial cells for polarity and basement membrane deposition. *J Cell Sci* 2002; **115**: 39–50.
36. Debnath J, Brugge JS. Modelling glandular epithelial cancers in three-dimensional cultures. *Nat Rev Cancer* 2005; **5**: 675–688.
37. Portillo-Lara R, Annabi N. Microengineered cancer-on-a-chip platforms to study the metastatic microenvironment. *Lab Chip* 2016; **16**: 4063–4081.
38. Santagata S, Thakkar A, Ergonul A, et al. Taxonomy of breast cancer based on normal cell phenotype predicts outcome. *J Clin Invest* 2014; **124**: 859–870.
39. Burdall SE, Hanby AM, Lansdown MR, et al. Breast cancer cell lines: friend or foe? *Breast Cancer Res* 2003; **5**: 89–95.
40. Qu Y, Han B, Yu Y, et al. Evaluation of MCF10A as a reliable model for normal human mammary epithelial cells. *PLoS One* 2015; **10**: e0131285.
41. Sachs N, de Ligt J, Kopper O, et al. A living biobank of breast cancer organoids captures disease heterogeneity. *Cell* 2018; **172**: 373–386.e10.
42. Linnemann JR, Meixner LK, Miura H, et al. An organotypic 3D assay for primary human mammary epithelial cells that recapitulates branching morphogenesis. *Meth Mol Biol* 2017; **1612**: 125–137.
43. Eirew P, Stingl J, Raouf A, et al. A method for quantifying normal human mammary epithelial stem cells with in vivo regenerative ability. *Nat Med* 2008; **14**: 1384–1389.
44. Wozniak MA, Keely PJ. Use of three-dimensional collagen gels to study mechanotransduction in T47D breast epithelial cells. *Biol Proced Online* 2005; **7**: 144–161.
45. Hu Y, Smyth GK. ELDA: extreme limiting dilution analysis for comparing depleted and enriched populations in stem cell and other assays. *J Immunol Methods* 2009; **347**: 70–78.
46. Rattan B, Manjari M, Kahlon SK, et al. The immunohistochemical expression of the oestrogen receptor (ER), HER-2/NEU and cytokeratin 8/18 and 5/6 in invasive breast carcinoma. *J Clin Diagn Res* 2012; **6**: 1495–1498.
47. Bell J, Walsh S, Nusrat A, et al. Zonula occludens-1 and Her-2/neu expression in invasive breast carcinoma. *Appl Immunohistochem Mol Morphol* 2003; **11**: 125–129.
48. Matsukita S, Nomoto M, Kitajima S, et al. Expression of mucins (MUC1, MUC2, MUC5AC and MUC6) in mucinous carcinoma of the breast: comparison with invasive ductal carcinoma. *Histopathology* 2003; **42**: 26–36.

49. Friedl P, Gilmour D. Collective cell migration in morphogenesis, regeneration and cancer. *Nat Rev Mol Cell Biol* 2009; **10**: 445–457.
50. Gudjonsson T, Villadsen R, Nielsen HL, *et al.* Isolation, immortalization, and characterization of a human breast epithelial cell line with stem cell properties. *Genes Dev* 2002; **16**: 693–706.
51. Zhou H, Kramer RH. Integrin engagement differentially modulates epithelial cell motility by RhoA/ROCK and PAK1. *J Biol Chem* 2005; **280**: 10624–10635.
52. Yu W, Shewan AM, Brakeman P, *et al.* Involvement of RhoA, ROCK I and myosin II in inverted orientation of epithelial polarity. *EMBO Rep* 2008; **9**: 923–929.
53. Winkler J, Abisoye-Ogunniyan A, Metcalf KJ, *et al.* Concepts of extracellular matrix remodelling in tumour progression and metastasis. *Nat Commun* 2020; **11**: 5120.
54. Provenzano PP, Eliceiri KW, Campbell JM, *et al.* Collagen reorganization at the tumor-stromal interface facilitates local invasion. *BMC Med* 2006; **4**: 38.
55. Provenzano PP, Inman DR, Eliceiri KW, *et al.* Contact guidance mediated three-dimensional cell migration is regulated by Rho/ROCK-dependent matrix reorganization. *Biophys J* 2008; **95**: 5374–5384.
56. Brownfield DG, Venugopalan G, Lo A, *et al.* Patterned collagen fibers orient branching mammary epithelium through distinct signaling modules. *Curr Biol* 2013; **23**: 703–709.
57. Friedl P, Wolf K. Tube travel: the role of proteases in individual and collective cancer cell invasion. *Cancer Res* 2008; **68**: 7247–7249.
58. Kessenbrock K, Plaks V, Werb Z. Matrix metalloproteinases: regulators of the tumor microenvironment. *Cell* 2010; **141**: 52–67.
59. Feinberg TY, Zheng H, Liu R, *et al.* Divergent matrix-remodeling strategies distinguish developmental from neoplastic mammary epithelial cell invasion programs. *Dev Cell* 2018; **47**: 145–160.e6.
60. Varner VD, Nelson CM. Cellular and physical mechanisms of branching morphogenesis. *Development* 2014; **141**: 2750–2759.
61. Friedl P, Locker J, Sahai E, *et al.* Classifying collective cancer cell invasion. *Nat Cell Biol* 2012; **14**: 777–783.
62. McCart Reed AE, Kutasovic JR, Lakhani SR, *et al.* Invasive lobular carcinoma of the breast: morphology, biomarkers and 'omics. *Breast Cancer Res* 2015; **17**: 12.
63. Budczies J, Bockmayr M, Denkert C, *et al.* Classical pathology and mutational load of breast cancer - integration of two worlds. *J Pathol Clin Res* 2015; **1**: 225–238.
64. Schipper K, Seinstra D, Paulien Drenth A, *et al.* Rebalancing of actomyosin contractility enables mammary tumor formation upon loss of E-cadherin. *Nat Commun* 2019; **10**: 3800.
65. Kalluri R. The biology and function of fibroblasts in cancer. *Nat Rev Cancer* 2016; **16**: 582–598.
66. Hanahan D, Weinberg RA. Hallmarks of cancer: the next generation. *Cell* 2011; **144**: 646–674.
67. Geraldo S, Simon A, Vignjevic DM. Revealing the cytoskeletal organization of invasive cancer cells in 3D. *J Vis Exp* 2013; **80**: e50763.
68. Buchmann B, Engelbrecht LK, Fernandez P, *et al.* Mechanical plasticity of collagen directs branch elongation in human mammary gland organoids. *Nat Commun* 2021; **12**: 2759.
69. Breunig CT, Durovic T, Neuner AM, *et al.* One step generation of customizable gRNA vectors for multiplex CRISPR approaches through string assembly gRNA cloning (STAgR). *PLoS One* 2018; **13**: e0196015.

References 67–69 are cited only in the supplementary material.

SUPPLEMENTARY MATERIAL ONLINE

Supplementary materials and methods

Supplementary figure legends

Figure S1. Human mammary luminal progenitor cells give rise to complex branched ductal structures in collagen type I gels

Figure S2. Branched luminal organoids are negative for basal lineage marker

Figure S3. Luminal progenitor-derived branched organoid formation requires inhibition of ROCK-myosin II signaling

Figure S4. Ductal organoids are generated through invasive branching morphogenesis

Figure S5. Deletion of E-cadherin results in ILC-like morphology

Table S1. Reduction mammoplasty donors

Table S2. Media composition (BCOM and BLOM) with respective concentrations

Table S3. Antibodies and cellular stains used for fluorescence activated cell sorting

Table S4. Primary antibodies used for immunofluorescence and blocking

Table S5. Secondary antibodies used for immunofluorescence

Movie S1. Displacement of fluorescent beads in the presence of ROCK inhibitor

Movie S2. Displacement of fluorescent beads in the absence of ROCK inhibitor

Movie S3. Duct elongation without marimastat treatment (control)

Movie S4. Inhibition of duct elongation upon marimastat treatment

Movie S5. Tip cell driven duct elongation

Movie S6. Tip cell exchange

Movie S7. Arising of new ducts via bifurcation

Movie S8. Dissolution of duct elongation upon HECD1 treatment